

Surface-Wave Coupling to Single Phononic Subwavelength Resonators

Sarah Benchabane,^{*} Roland Salut, Olivier Gaiffe, Valérie Soumann, Mahmoud Addouche, Vincent Laude, and Abdelkrim Khelif

Institut FEMTO-ST, CNRS, Université de Bourgogne Franche-Comté 15B Avenue des Montboucons, F-25030 Besançon Cedex, France

(Received 1 February 2017; revised manuscript received 23 June 2017; published 21 September 2017)

We propose to achieve manipulation of mechanical vibrations at the micron scale by exploiting the interaction of individual, isolated mechanical resonators with surface acoustic waves. We experimentally investigate a sample consisting of cylindrical pillars individually grown by focused-ion-beam-induced deposition on a piezoelectric substrate, exhibiting different geometrical parameters and excited by a long-wavelength surface elastic wave. The mechanical displacement is strongly confined in the resonators, as shown by field maps obtained by laser scanning interferometry. A tenfold displacement field enhancement compared to the vibration at the surface is obtained, revealing that the energy is efficiently coupled. The spatial distribution of the elastic energy at the surface is governed by the geometrical characteristics of the resonators and can therefore be controlled by frequency tuning the elastic wave source. The results show the potential of the proposed approach to achieve dynamic control of surface phonons at the microscale or nanoscale.

DOI: [10.1103/PhysRevApplied.8.034016](https://doi.org/10.1103/PhysRevApplied.8.034016)

I. INTRODUCTION

In this era of microtechnology and nanotechnology, mechanical resonators have again emerged as rich physical objects at the core of thriving research fields such as micro- and nano-electro-mechanical systems or optomechanics [1–3]. This resurgence of interest has been partly motivated by the possibility to fabricate microscale or nanoscale resonators with tailorable properties. In addition to their obvious use as low-mass objects allowing for the realization of highly sensitive detectors ranging from motion sensors or accelerometers to chemical or biological detectors, mechanical resonators open exciting vistas for the investigation of basic quantum-mechanical concepts [4–6]. They have also made their way toward phononics where they lie at the heart of acoustic or elastic metamaterials. Acoustic local resonances were first introduced as a way to obtain phononic band gaps at frequencies significantly lower than those induced by Bragg diffraction for an equally sized crystal period [7]. Since then, the phononic-crystal literature has witnessed significant progress in the understanding of the hybridization mechanisms underlying the coupling between resonant scatterers and waves propagating in the surrounding continuous medium in both classical periodical phononic crystals and disordered media. This concept has been applied to surface acoustic waves (SAW), for instance to investigate contact resonance effects at the micron scale in granular materials [8,9] or band-gap properties and hybridization mechanisms in locally resonant SAW phononic crystals [10,11]. These approaches can be seen as extensions of earlier works

exploiting coupling between SAWs and arrays of mechanical surface resonators to slow down wave propagation by creating corrugations on the surface of the substrate [12]. Theoretical investigations of the interaction between propagating Rayleigh waves with mechanical oscillators randomly distributed on the surface have shown interesting dispersion characteristics, including anticrossings due to mode repulsion resulting from coupling of the surface wave with the resonator eigenmodes [13]. These features are very close to those observed when considering surface plasmon polaritons at single interface [14]. In acoustics or phononics, however, the local resonance concept has mostly been tackled as a way to control wave propagation through a collection of resonators, and works dealing with resonant elements are scarce [15]. The interaction of isolated resonators with a supporting surface is usually considered in the light of micromechanics where it is seen as an intense source of losses and considered as detrimental. Yet, similarly to what has been achieved in plasmonics [16], such an approach could make it possible to conceive phononic chains capable of carrying the elastic energy in subwavelength structures. Here, we experimentally demonstrate that resonator-to-surface coupling can be deliberately used to excite discrete micron-scale mechanical resonators and to confine elastic energy. Using focused-ion-beam-induced deposition (FIBID), we fabricate sets of isolated cylindrical pillars of independent, arbitrary shapes and sizes to investigate the possibility of coupling surface acoustic waves propagating on the homogeneous substrate with each resonator independently. This coupling occurs through a hybridization mechanism of the supporting continuum with the resonator eigenmodes. The sample considered comprises cylindrical pillars 3–5 μm in diameter excited by a

^{*}sarah.benchabane@femto-st.fr

ten-times longer wavelength surface elastic wave. The elastic field distributions in the resonators and at the substrate surface are characterized by laser scanning interferometry, a method that allows a direct visualization of the out-of-plane component of the displacement field. This experiment is used to demonstrate that the elastic energy distribution at the substrate surface can be dynamically controlled at a subwavelength scale by addressing each resonator independently as a function of the elastic wave-source frequency.

II. RESONATOR FABRICATION AND ELASTIC SOURCE INTEGRATION

The resonators shown in Fig. 1 are platinum-based cylindrical pillars fabricated by FIBID, a unique technology providing a full control, along the three space dimensions and with nanometer accuracy, of the fabricated structures [17,18]. FIBID allows us to control individually the geometrical parameters of each pillar, making this process particularly well suited for the fabrication of complex systems of isolated resonators exhibiting different shapes and sizes on the same substrate. An FEI Helios Nanolab 600i Dualbeam FIB-SEM system is then used to produce seven pillars with diameters and heights ranging from 3 to 5 μm . The pillars are grown on a bulk piezoelectric substrate, here a 500- μm -thick LiNbO₃ wafer in the *Y*-crystallographic orientation, to ensure electroacoustic transduction through direct integration of elastic wave sources. The choice of resonator dimensions is driven by the need to distinctly map the displacement field at the

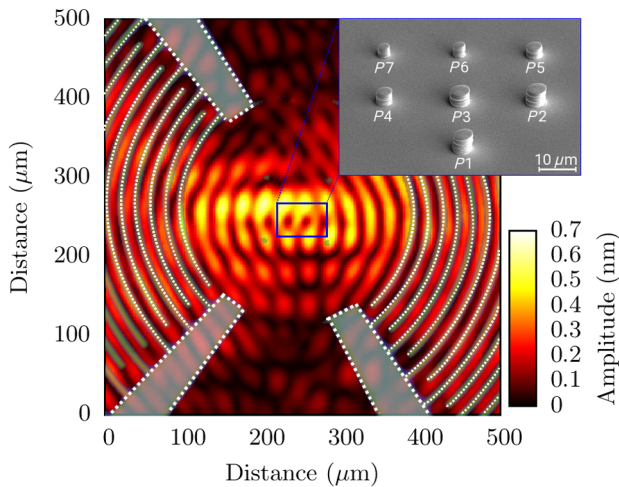


FIG. 1. Measurement of the out-of-plane component of the displacement field generated by a chirped annular interdigitated transducer for an excitation frequency of 75 MHz. A microscope picture of the fingers and pads overlays the measurement data as a guide for the eye. Inset: scanning-electron-microscope image of the fabricated pillars. The geometrical dimensions of pillars P1 to P7 are as follows: diameter $d = [5.1, 5.1, 5.2, 4.2, 4.0, 3.1, 3.2] \mu\text{m}$; height $h = [5.2, 4.7, 3.9, 3.7, 3.2, 3.6, 3.0] \mu\text{m}$.

pillar surface using optical interferometry in order to retrieve the resonance mode shape. The pillar height is subsequently defined through finite element simulations, further detailed in Sec. IV, to allow operation above 50 MHz and to ensure that we remain well in the Rayleigh wave regime given the substrate thickness. A gas injection system dedicated to platinum deposition is used to locally inject the trimethyl-(methylcyclopentadienyl)-platinum(IV) precursor on the sample. The pillars are grown with an accelerating voltage of 30 kV and a probe current of 40 pA, carefully chosen to limit the roughness of the structures on the sidewalls and on the top surface. The atomic composition of the deposited material is characterized by energy-dispersive x-ray spectroscopy showing a ratio of 53% of platinum, 18% of gallium, and 29% of carbon.

A scanning-electron-microscope (SEM) image of the resulting sample is reported in Fig. 1. The surface of the pillars is tilted with an angle of about 7° with respect to the substrate surface. This tilt angle is partly due to the injection nozzle position during the growth process. The distance between adjacent pillars is 20 μm , large enough to avoid potential coupling between neighboring resonators.

Broadband interdigitated transducers (IDTs) are used for SAW generation at the substrate surface. In their most classical form, IDTs consist of interleaved periodic metal electrodes deposited atop a piezoelectric substrate. Excitation of the pillar array requires a wide band operation that can be achieved by chirping the IDT period at the expense, however, of the displacement field amplitude for each frequency component [19]. To partially overcome this limitation, we propose to focus the elastic energy through the use of quasiannular interdigitated transducers (AIDTs) based on the principle reported in Ref. [20] designed so that the electrode shape follows the elastic wave surface. We focus in the present work on the generation of Rayleigh waves with sagittal polarization. The fabricated transducers then consist of 200-nm-thick aluminum electrodes designed to operate at a wavelength ranging from 34 to 68 μm , leading to a center frequency equal to 70 MHz and a relative emission bandwidth of 75% expected to cover the required frequency range. Figure 1 shows a typical displacement field distribution obtained by laser scanning interferometry, here given for an excitation frequency of 75 MHz. The scan covers an area of 500 $\mu\text{m} \times 500 \mu\text{m}$ with a 2- μm step size. Convergence of surface waves at the center of the transducer is clearly obtained. The area of interest that hosts the pillar array is therefore illuminated by a broadband stationary elastic wave source with a maximum amplitude of displacement of the order of 1 nm.

III. COUPLING OF ELASTIC ENERGY IN DISCRETE PHONONIC RESONATORS

The fabricated platinum pillars can be seen as discrete mechanical resonators deposited on the surface. The shear

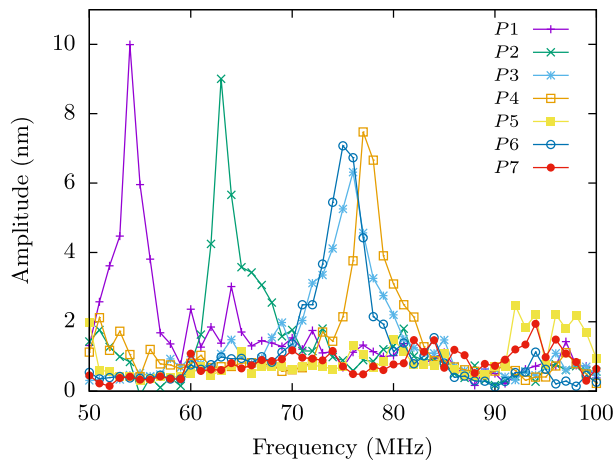


FIG. 2. Frequency response of the fabricated pillars, obtained by retrieving the maximum amplitude of vibration of each resonator as a function of excitation frequency. The frequency step is 1 MHz.

mechanical contact between resonator and substrate makes the system radiative. We aim here at showing that it is anyway possible to couple and confine the elastic energy inside the resonator through hybridization of the pillars' eigenmodes with the supporting continuum.

Although the compression mode is most probably the easiest to investigate using optical heterodyne interferometry, as the corresponding displacement field is only polarized in the out-of-plane direction, we choose to focus on the first flexural mode, for which radiation to the bulk is intrinsically low because of the dipolar character induced by modal symmetry. The response of the mechanical resonators is, therefore, measured via optical interferometry over the entire transducer emission band with 1-MHz steps. The maximum amplitude of vibration as a function of excitation frequency for all seven pillars is displayed in Fig. 2. Each resonator responds at a specific frequency dictated by the geometrical characteristics of the fabricated structures. Five out of seven pillars exhibit a clear response in the frequency range of interest. The vibration amplitude of *P5* and *P7* is seven-to-eight times lower, as their resonance frequency is very close to the emission edge of the surface acoustic-wave source. For pillars *P1* to *P4* and *P6*, the out-of-plane displacement is of the order of 8–10 nm for a maximum of 1 nm at the substrate surface. There is, therefore, a seven-to-tenfold increase in amplitude, compared to the one measured for the incident Rayleigh wave. An estimation of the typical quality factor Q of such resonators is obtained by refining the measurements performed on pillar *P1* by setting the frequency acquisition step to 100 kHz. Figure 3 displays the corresponding data. The quality factor is estimated to be about 40, as inferred from nonlinear least-square fitting of the experimental data with a Lorentzian line shape, hence leading to a quality factor and frequency product ($Q - f$) of the order of 10^9 Hz at room temperature and ambient pressure. This value may be limited by the resonator

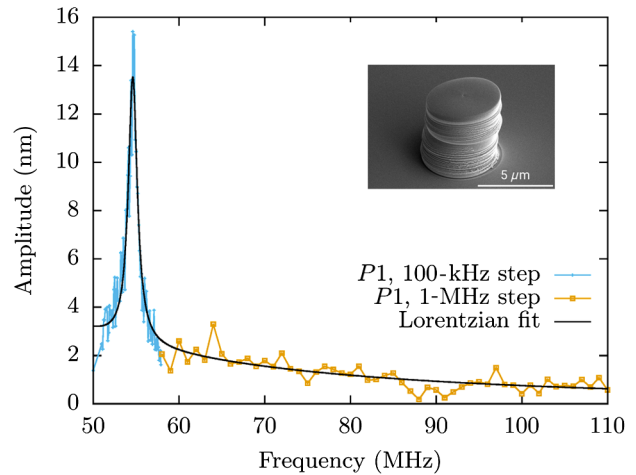


FIG. 3. Frequency response of pillar *P1*, obtained by retrieving the maximum amplitude of vibration as a function of excitation frequency. The frequency step is refined to 100 kHz around the resonance, while a 1-MHz step is used outside resonance. The associated Lorentzian fit, displayed in the dotted line, leads to a quality factor of 43 ± 3 . Inset: scanning-electron-microscope image of pillar *P1*.

roughness and geometrical irregularities, in particular by the overall structure and top surface tilts that break the resonator symmetry, as illustrated by the SEM image featured as the inset in Fig. 3.

Figure 4 presents the displacement field maps obtained for excitation frequencies of 54, 77, and 95 MHz, corresponding to the resonance frequencies of pillars *P1*, *P3-P4*, and *P7*, respectively. The first two frequencies are well within the AIDT operation range; 95 MHz is at the edge of the transducer bandwidth. A significant elastic field enhancement in the pillar with respect to the surface is revealed by the measurements, showing that the elastic energy can be efficiently coupled through the substrate surface in the resonators under potentially radiative conditions. The pillars are addressed independently as a function of drive frequency: the ability to control individually the geometrical properties of the resonators further provides a direct way to control dynamically the energy distribution at the substrate surface. The vibration at the pillar surface features a nodal line at the center, as expected for a first-order flexural mode, further highlighted by the cross section of the displacement field amplitude at 54 MHz. This observation suggests that the excited mechanical resonances correspond to natural eigenmodes of the phononic resonators.

IV. NUMERICAL MODELING

To relate the excited mechanical resonances to eigenmodes of the pillars, two numerical models are implemented and compared. The first one consists of solving a simple eigenvalue problem. The model considers a Pt cylinder deposited on a lithium-niobate substrate consisting of a half sphere of a diameter equal to half a wavelength with

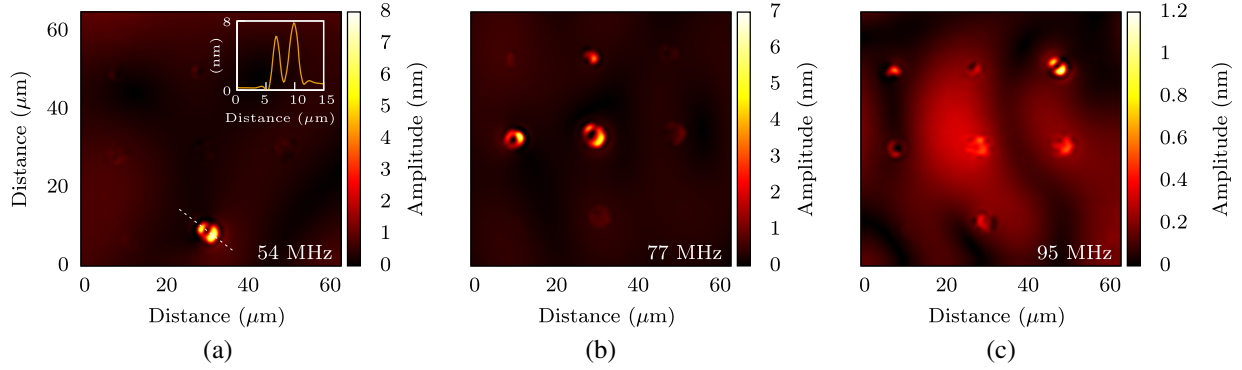


FIG. 4. Out-of-plane displacement for excitation frequencies of (a) 54 MHz, (b) 77 MHz, and (c) 95 MHz. The scans cover an area of $60 \mu\text{m} \times 60 \mu\text{m}$ with a $0.5\text{-}\mu\text{m}$ step size. Inset of (a), cross section of the vibration amplitude for pillar *P1* along the dotted line.

clamped boundary conditions at the bottom. The second model implements a time-harmonic excitation of a pillar deposited over a rectangular-shaped substrate. The model integrates perfectly matched layers on the four sides and at the bottom of the computation domain to absorb radiation to the bulk. An external, circular line source presenting all three polarizations is placed in the near field of the resonator and used as an excitation signal. The two models rely on the finite element method, through the COMSOL MULTIPHYSICS software, and take into account anisotropy and piezoelectricity of the substrate. In both cases, a density of 10^4 kg m^{-3} , inferred from independent characterizations, is used to perform the computations; the Young's modulus and the Poisson coefficient are set to 130 GPa and 0.38, respectively.

Solving the eigenvalue problem first allows identifying typical eigenmodes and eigenfrequencies expected for such low-aspect-ratio mechanical resonators. An example of a parametric sweep obtained for a pillar with a diameter of

$d = 3.1 \mu\text{m}$ and a varying height is displayed in Fig. 5. The eigenfrequencies of the first three modes along with the corresponding mode shapes are reported. The first mode is a flexural mode with eigenfrequencies ranging between 40 and 120 MHz, depending on the pillar height. The second mode is a purely in-plane mode, appearing at frequencies of the order of 140 MHz for a $3\text{-}\mu\text{m}$ -high pillar. The third one is a compression mode, with an essentially out-of-plane polarization and strong coupling to the bulk. This mode would appear at frequencies of about 180 MHz in the range of dimensions corresponding to the fabricated resonators. The first flexural mode is therefore the only eigenmode responding in the frequency range of the elastic wave source used in the experiments. Time-harmonic simulations are then performed and compared to eigenvalue solving to determine whether the experimentally observed resonances are indeed due to a hybridization of a pillar eigenmode with an elastic wave excited through the surface. First, the resonance frequencies of the flexural mode for all fabricated pillars are calculated using both numerical models. The obtained results are reported in Table I. The good agreement on the resonance frequencies obtained through the two simulation methods is expected: radiation to the bulk substrate is intrinsically low for the first flexural mode, which makes it less sensitive to reflections caused by the

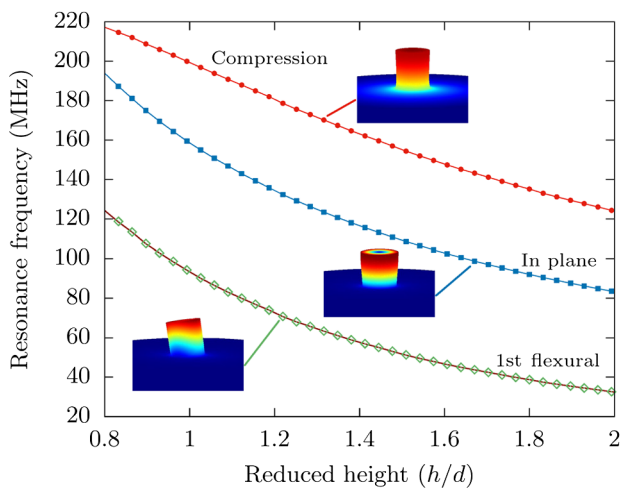


FIG. 5. Simulated eigenfrequencies of the first free natural modes of a $3.1\text{-}\mu\text{m}$ -diameter pillar as a function of pillar height. The corresponding computed total field distributions are given in the insets.

TABLE I. Comparison between experimental resonance frequencies (exp), eigenfrequencies (ef) and obtained through time-harmonic simulations (TH). The Young's modulus is set to 130 GPa, the Poisson's ratio to 0.38.

Pillar	d (μm)	h (μm)	$f_{\text{res exp}}$ (MHz)	$f_{\text{res ef}}$ (MHz)	$f_{\text{res TH}}$ (MHz)
<i>P1</i>	5.1	5.2	54	56	56
<i>P2</i>	5.1	4.7	63	64	64
<i>P3</i>	5.2	3.9	76	81	81
<i>P4</i>	4.2	3.7	78	82	81.5
<i>P5</i>	4	3.2	...	98	97
<i>P6</i>	3.1	3.6	75	76	76.5
<i>P7</i>	3.2	3	94	100	99

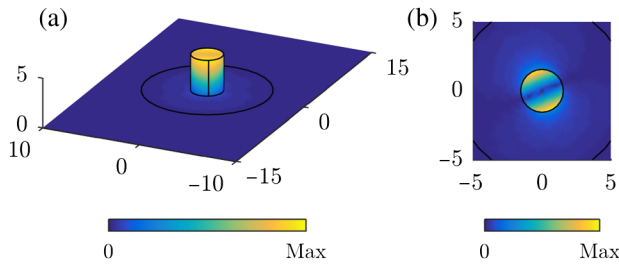


FIG. 6. (a) Total displacement distribution obtained by finite element simulations for pillar *P6*. The resonator is excited by a circular line source with displacements along the three possible polarization directions. (b) Out-of-plane component of the displacement field. All dimensions are in millimeters.

clamped boundary condition at the bottom of the computational domain. This characteristic probably accounts for the fair accordance observed between experimentally measured and numerically simulated resonance frequencies. The elastic energy distribution in the pillar and on the surrounding surface is then calculated through time-harmonic simulations. As an example, Fig. 6 displays the distribution of the total displacement and of the out-of-plane component of the displacement field for pillar *P6* (diameter $d = 3.1 \mu\text{m}$ and height $h = 3.6 \mu\text{m}$) at resonance ($f = 75 \text{ MHz}$). The numerically obtained energy distribution exhibits a clear nodal line that corresponds well to the one optically measured. These simulations then confirm that the experimentally measured vibrations correspond to intrinsic flexural modes of the mechanical resonator excited through the substrate surface.

V. ELASTIC ENERGY CONFINEMENT IN SUBWAVELENGTH PHONONIC RESONATORS

Both experimental elastic field maps and numerical simulations point at a tight confinement of the elastic energy in the proposed subwavelength resonators. To support these observations, an additional sample hosting a single pillar is fabricated and characterized. The resonator now exhibits a diameter of $3.2 \mu\text{m}$, a height of $3.3 \mu\text{m}$, and is again excited with a surface wave emitted by an AIDT. The obtained measurements are opposed to characterizations of the elastic field performed on a reference, pillar-free sample.

Figure 7 reports the maximum amplitude measured at the surface for different radial distances x from the pillar center. Elastic field maps are first taken at different excitation frequencies. Circles of increasing radius are created on each field map, taking the pillar center as the centroid. The maximum amplitude outside each circle is then extracted to build the data set used for Fig. 7. It should be noted here that as the laser probe spot size is $1.5 \mu\text{m}$, the data only become significant when the radial distance is at least half a spot size away from the pillar edge, or $2.25 \mu\text{m}$ from the center. For smaller distances, the spot size and the scanning

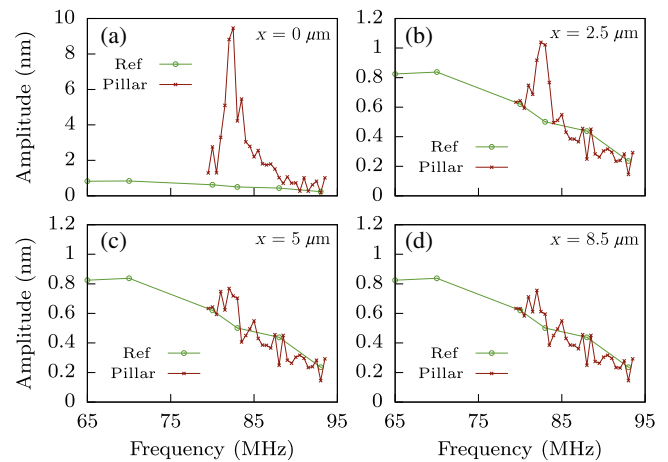


FIG. 7. Displacement amplitude measured at the surface of a substrate hosting a $3.2\text{-}\mu\text{m}$ -diameter, $3.3\text{-}\mu\text{m}$ -high Pt pillar, obtained by retrieving the maximum amplitude of vibration as a function of excitation frequency and measured at different radial distances x to the pillar center (respectively, $x = 0, 2.5, 5,$ and $8.5 \mu\text{m}$). The response of the surface elastic wave excitation source obtained from a pillar-free sample is given as a reference.

step lead to an integration of the signal including a direct contribution from the pillar.

Figure 7(a) (label $x = 0$) corresponds to an extraction performed strictly on the pillar. The frequency response of the resonator therefore shows an amplitude of vibration at a resonance of the order of 9 nm , a value comparable to those obtained for the pillar ensemble previously discussed. The measured resonance frequency is about 82.5 MHz , while numerical simulations predict a frequency of about 86 MHz . At a radial distance of $2.5 \mu\text{m}$ from the pillar center [i.e., $1 \mu\text{m}$ from the pillar edge, Fig. 7(b)], the displacement field amplitude is about 1 nm , versus 0.77 nm for the free surface. At $5 \mu\text{m}$ from the pillar center, the amplitude is at the same level as the one measured for the pillar-free sample and the pillar no longer contributes to the elastic energy distribution at the substrate surface. This trend is confirmed as the radial distance increases, as shown in Fig. 7(d), corresponding to a distance of $8.5 \mu\text{m}$.

In order to evaluate precisely the energy decrease outside the resonator, time-harmonic numerical simulations are performed and compared to experimental data. Cross sections of the modeled elastic energy distribution of the out-of-plane component of the displacement field are reported in Fig. 8(a). The two-dimensional cross section clearly shows that the pillar acts as a secondary dipolar elastic wave source with limited radiation towards the bulk. A cross section taken in the direction orthogonal to the nodal line confirms the strong energy decrease outside the resonator. The displacement amplitude reaches a maximum at the pillar edge and the elastic energy decays exponentially outside of the pillar, leading to an amplitude level tending toward zero at a distance of about $8 \mu\text{m}$ from the pillar center when removing the contribution of the surface

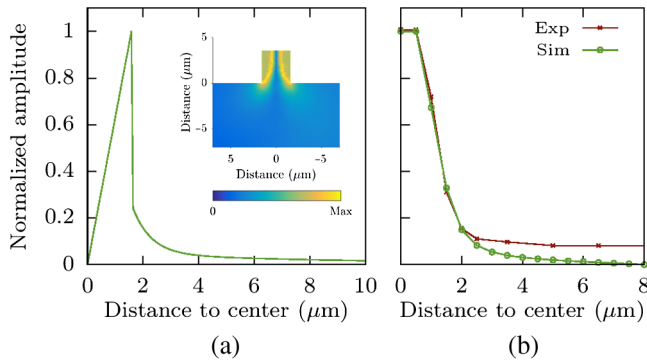


FIG. 8. Elastic energy decay at the substrate surface as a function of distance to pillar center: (a) Simulation results obtained by cross sectioning the elastic field maps obtained through time-harmonic simulations. The two-dimensional cross section in the inset shows the spatial distribution of the elastic energy within the pillar and beneath the substrate surface. (b) Comparison between experimental measurements and numerically convoluted simulation data.

acoustic-wave excitation source. The image of the computed surface-wave field-map distribution is then numerically convoluted by a $1.5\text{-}\mu\text{m}$ -diameter Gaussian spot, assuming a 500-nm step size. In Fig. 8(b), the resulting one-dimensional normalized cross section is compared with experimental data. The higher displacement amplitude measured at the substrate surface at a few micrometer distance from the pillar corresponds to the contribution of the impinging surface acoustic-wave source. Regardless of this feature, there is a clear match between the two sets of data. The displacement amplitude measured outside the pillar, therefore, tends to the one at the free surface within a distance much lower than the characteristic wavelength of the excitation signal. This further confirms the absence of intrinsic coupling between resonators in the pillar ensemble, supporting the achievement of a tight control of the spatial distribution of the elastic energy by a careful arrangement of phononic resonators.

VI. CONCLUSION

In conclusion, we have experimentally demonstrated the possibility of coupling independently elastic energy in individual mechanical resonators excited by a long-wavelength surface acoustic wave. The elastic energy is efficiently confined in micron-scale cylindrical pillars, leading to an energy localization in dimensions at least ten times smaller than the excitation wavelength. A strong field enhancement as compared to the one hosted by the wave propagating on the substrate surface is reported. The pillars are fabricated individually using FIBID, a technological process that intrinsically allows a three-dimensional control of the resonator geometrical properties at an individual level. The proposed experimental configuration is therefore used to show that the spatial distribution of the

elastic energy at the substrate surface can be controlled by addressing each pillar independently as a function of drive frequency, hence opening the door for coherent, high-frequency elastic wave distribution and confinement at the microscale or nanoscale. Potential outcomes may lie in devices with acousto-optical or acoustoplasmonic functionalities or in charge transport.

ACKNOWLEDGMENTS

This work was supported by the Agence Nationale de la Recherche under Grant No. ANR-14-CE26-0003-01-PHOREST and through LabEx ACTION (ANR-11-LABX-0001-01) and by the Région de Franche-Comté. The authors also acknowledge partial support of the French RENATECH network and its FEMTO-ST technological facility.

- [1] H. G. Craighead, Nanoelectromechanical systems, *Science* **290**, 1532 (2000).
- [2] K. L. Ekinci and M. L. Roukes, Nanoelectromechanical systems, *Rev. Sci. Instrum.* **76**, 061101 (2005).
- [3] M. Aspelmeyer, T. J. Kippenberg, and F. Marquardt, Cavity optomechanics, *Rev. Mod. Phys.* **86**, 1391 (2014).
- [4] K. C. Schwab and M. L. Roukes, Putting mechanics into quantum mechanics, *Phys. Today* **58**, 36 (2005).
- [5] M. Li, H. X. Tang, and M. L. Roukes, Ultra-sensitive NEMS-based cantilevers for sensing, scanned probe and very high-frequency applications, *Nat. Nanotechnol.* **2**, 114 (2007).
- [6] J. D. Teufel, T. Donner, D. Li, and J. W. Harlow, Sideband cooling of micromechanical motion to the quantum ground state, *Nature (London)* **475**, 359 (2011).
- [7] Z. Liu, X. Zhang, Y. Mao, Y. Y. Zhu, Z. Yang, C. T. Chan, and P. Sheng, Locally resonant sonic materials, *Science* **289**, 1734 (2000).
- [8] N. Boechler, J. K. Eliason, A. Kumar, A. A. Maznev, K. A. Nelson, and N. Fang, Interaction of a Contact Resonance of Microspheres with Surface Acoustic Waves, *Phys. Rev. Lett.* **111**, 036103 (2013).
- [9] M. Hiraiwa, M. Abi Ghanem, S. P. Wallen, A. Khanolkar, A. A. Maznev, and N. Boechler, Complex Contact-Based Dynamics of Microsphere Monolayers Revealed by Resonant Attenuation of Surface Acoustic Waves, *Phys. Rev. Lett.* **116**, 198001 (2016).
- [10] Y. Achouai, A. Khelif, S. Benchabane, L. Robert, and V. Laude, Experimental observation of locally-resonant and Bragg band gaps for surface guided waves in a phononic crystal of pillars, *Phys. Rev. B* **83**, 104201 (2011).
- [11] D. Yulistira, A. Boes, B. Graczykowski, F. Alzina, L. Y. Yeo, C. M. Sotomayor Torres, and A. Mitchell, Nanoscale pillar hypersonic surface phononic crystals, *Phys. Rev. B* **94**, 094304 (2016).
- [12] B. Auld and J. Gagnepain, Horizontal shear surface waves on corrugated surfaces, *Electron. Lett.* **12**, 650 (1976).

- [13] E. A. Garova, A. A. Maradudin, and A. P. Mayer, Interaction of Rayleigh waves with randomly distributed oscillators on the surface, *Phys. Rev. B* **59**, 13291 (1999).
- [14] S. Maier, *Plasmonics: Fundamentals and Applications* (Springer, New York, 2007).
- [15] V. P. Plesky and A. W. Simonian, Rayleigh wave reflection and scattering on a resonator, *Phys. Lett. A* **155**, 281 (1991).
- [16] E. Ozbay, Plasmonics: Merging photonics and electronics at nanoscale dimensions, *Science* **311**, 189 (2006).
- [17] S. Matsui, T. Kaito, J.-I. Fujita, M. Komuro, K. Kanda, and Y. Haruyama, Three-dimensional nanostructure fabrication by focused-ion-beam chemical vapor deposition, *J. Vac. Sci. Technol. B* **18**, 3181 (2000).
- [18] S. Reyntjens and R. Puers, Focused ion beam induced deposition: Fabrication of three-dimensional microstructures and Young's modulus of the deposited material, *J. Micromech. Microeng.* **10**, 181 (2000).
- [19] D. Morgan and E. Paige, in *Surface Acoustic Wave Filters*, 2nd ed., edited by D. Morgan and E. Paige, Studies in Electrical and Electronic Engineering (Academic Press, Oxford, 2007), pp. 183–224.
- [20] V. Laude, D. Gérard, N. Khelifaoui, C. F. Jerez-Hanckes, S. Benchabane, and A. Khelif, Subwavelength focusing of surface acoustic waves generated by an annular interdigital transducer, *Appl. Phys. Lett.* **92**, 094104 (2008).